

Chemical Science

Accepted Manuscript

This article can be cited before page numbers have been issued, to do this please use: E. Sebastian, D. G. Congrave, J. Royakkers, S. Montanaro, H. Huang, A. Sharma, J. Osmólska, H. Zhu, C. Phansa, J. F. Winkel, O. Millington, M. J. Y. Tayebjee, L. Campos, H. Bronstein and A. Rao, *Chem. Sci.*, 2026, DOI: 10.1039/D6SC00278A.



This is an Accepted Manuscript, which has been through the Royal Society of Chemistry peer review process and has been accepted for publication.

Accepted Manuscripts are published online shortly after acceptance, before technical editing, formatting and proof reading. Using this free service, authors can make their results available to the community, in citable form, before we publish the edited article. We will replace this Accepted Manuscript with the edited and formatted Advance Article as soon as it is available.

You can find more information about Accepted Manuscripts in the [Information for Authors](#).

Please note that technical editing may introduce minor changes to the text and/or graphics, which may alter content. The journal's standard [Terms & Conditions](#) and the [Ethical guidelines](#) still apply. In no event shall the Royal Society of Chemistry be held responsible for any errors or omissions in this Accepted Manuscript or any consequences arising from the use of any information it contains.

ARTICLE

Controlling Triplet-Pair Formation in Acene-Bridged Trimers through Locally Excited–Charge-Transfer State Mixing

Ebin Sebastian^a, Daniel G. Congrave^{b,c†}, Jeroen Royakkers^{b†}, Stephanie Montanaro^b, Huaxi Huang^d, Ashish Sharma^a, Julia Osmólska^a, He Zhu^b, Chanakarn Phansa^a, Jurjen Winkel^a, Oliver Millington^b, Murad J. Y. Tayebjee^e, Luis M. Campos^d, Hugo Bronstein^{*a,b}, Akshay Rao^{*a}Received 00th January 20xx,
Accepted 00th January 20xx

DOI: 10.1039/x0xx00000x

Singlet fission (SF) offers a pathway to surpass conventional efficiency limits in photovoltaics, yet how bridge–chromophore coupling governs locally excited/charge-transfer state (LE-CT) mixing and thereby the multiexciton yield remains elusive. We design three systems, TIPS-BTO, TIPS-TAT, and Encap-TAT, that progressively increase bridge–chromophore coupling. Steady-state spectroscopy and transient absorption reveal that TIPS-BTO and TIPS-TAT undergo efficient SF, forming correlated triplet pairs (¹TT) and, in TIPS-TAT, long-lived triplets. By contrast, Encap-TAT loses vibronic structure and relaxes ultrafast into a broad, red-shifted intramolecular exciplex-like (Ex) state. Quantum chemical analysis shows that Ex state originates from strong hybridization between local excitations (LE) and bridge–chromophore CT configurations, driven by large electron and hole transfer integrals and a small LE-CT energy gap. Such strong LE-CT hybridisation suppresses well-defined ¹TT formation, favouring intramolecular Ex emission and enhancing photoluminescence quantum yield (≈80.5% vs. ≈38.5% for TIPS-TAT). These findings establish a unifying framework in which the balance between multiexciton generation and exciplex emission in acene-bridged trimers is governed by the degree of LE-CT mixing. Tuning bridge energetics and LE-CT offsets enable deliberate routing of excited-state pathways toward efficient triplet production or bright exciplex emission, providing actionable design rules for next-generation singlet-fission and optoelectronic architectures.

Introduction

Singlet fission (SF) is a spin-conserving multiexciton generation process in which one singlet exciton (S_1) splits into two triplet excitons (T_1), potentially doubling the exciton yield per absorbed photon and enabling photovoltaics to transcend the Shockley-Queisser limit.^{1–5} Although crystalline acenes and their derivatives first show cased intermolecular SF, their limited exciton diffusion, aggregation, and heterogeneous packing hinder practical device integration.^{6–8} In contrast, covalent intramolecular SF (iSF) molecules and polymers have emerged as a powerful alternative, offering precise control over geometry, solution processability, and electronic coupling between chromophores (Figure 1a).^{9–18}

A central challenge in iSF design lies in balancing electronic interactions. The chromophores must couple strongly enough

to form a correlated triplet pair (¹TT), yet remain sufficiently decoupled to allow triplet separation and avoid losses to excimer or charge-transfer (CT) traps.^{19–23} π -Conjugated bridges are therefore widely employed, not only to enforce distance and connectivity^{12,20,24–28} but also to actively tune the electronic landscape through resonance with chromophore frontier orbitals.^{29–31} Strategies spanning phenylene spacers, extended acenes, and macrocyclic frameworks have been explored to tailor molecular geometry, connectivity, and coupling (Figure 1a).^{13,32–39} In particular, rigid macrocyclic/cyclophane platforms enable precise cofacial arrangements that tune electronic coupling, giving singlet fission with strongly geometry-dependent rates and, in some cases, long-lived multiexciton signatures.^{40–43}

From a singlet-fission perspective, however, the role of CT-mediated interactions is nuanced. Moderate exciton–CT hybridisation can be advantageous, lowering the barrier to accessing CT-mediated ¹TT configurations and facilitating spin-space decoherence required for triplet separation (Figure 1b).^{26,34–36,44–46} Yet excessive CT admixture can destabilize the ¹TT channel, funneling population into excimer-like manifolds that suppress free-triplet yield.^{47–50} Particularly intriguing are cases where CT states localized on the bridge–chromophore axis hybridize with the local excitation of the fission-active unit. Such mixing may open superexchange pathways into ¹TT, or, if too strong, collapse the exciton into a delocalized LE-CT hybrid that bypasses multiexciton formation. Despite extensive

^a Cavendish Laboratory, University of Cambridge, Cambridge, CB3 0HE, United Kingdom.

^b Yusuf Hamied Department of Chemistry, University of Cambridge, Cambridge, CB2 1EW, United Kingdom

^c Chemistry Research Laboratory, University of Oxford, Oxford, OX1 3TA, United Kingdom.

^d Department of Chemistry, Columbia University, New York, New York 10027, United States.

^e School of Photovoltaic and Renewable Energy Engineering UNSW Sydney, Sydney, 2052, NSW, Australia

[†] These authors contributed equally.

Supplementary Information available: [details of any supplementary information available should be included here]. See DOI: 10.1039/x0xx00000x



ARTICLE

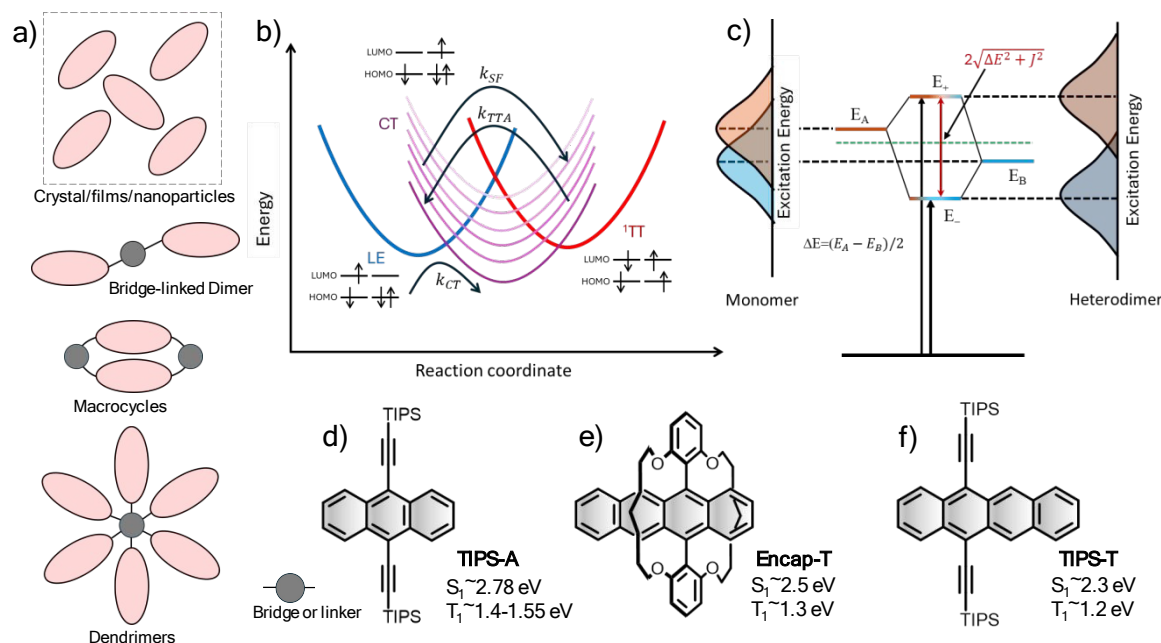


Figure 1. a) Molecular design strategies employed to achieve both intermolecular and intramolecular singlet fission, highlighting the transition from crystalline packing motifs to covalently bound multichromophoric scaffolds. b) Schematic illustration showing intramolecular singlet fission with a charge-transfer (CT) state. The bright local exciton LE (blue) is coupled to a ladder of CT states (violet tones) whose relative energy shifts with solvent polarity, and to the correlated triplet pair (¹TT) (red). When the CT level is strongly stabilized, it behaves as a population trap (rate k_{CT}); when it remains off-resonant it serves as a virtual superexchange mediator, enhancing LE → ¹TT conversion (rate k_{SF}). The same channel can also assist triplet–triplet annihilation back toward singlet character (rate k_{TTA}). c) Energy level diagram depicting exciton coupling between two distinct chromophores (A and B), where mixing leads to the formation of new hybrid excitonic states (E_+ and E_-), separated by an energy splitting proportional to $E_{A^+ E_B}/2 \pm \sqrt{\Delta E^2/2 + J^2}$; here, ΔE is the energy mismatch, and J is the electronic coupling. (d, e, f) Chemical structures of the SF chromophores and bridges used in this study, along with their estimated singlet and triplet energies (S_1 and T_1 , respectively), establish the energetic prerequisites for efficient intramolecular singlet fission.

efforts to tune electronic coupling through bridge design, the impact of bridge–chromophore resonance on LE–CT mixing and its consequences for singlet fission is not fully understood.

To address this gap, we employ a trimeric chromophore–bridge–chromophore scaffold as a minimal platform to tune LE–CT mixing while preserving a well-defined intramolecular SF motif on the terminal tetracenes. Relative to directly linked dimers, the bridge provides an independent handle over CT energetics and transfer integrals.^{35,51} It can also modulate the triplet–triplet exchange interaction that governs whether ¹TT remains bound or separates into long-lived triplets. TIPS-anthracene (**TIPS-A**) was chosen as the bridge because its higher triplet energy avoids acting as a triplet sink or heterofission channel, while its conjugated framework enables systematic control of electronic communication and CT-mediated superexchange. We further introduce Encap-tetracene (**Encap-**

T) to reduce LE–CT detuning and increase bridge–chromophore resonance while preventing aggregation and improving solubility.⁵² Accordingly, **TIPS-TAT** features a large CT–LE offset ($E_{CT} \approx 3.05$ eV; $E_{LE} \approx 2.30$ eV; $\Delta E_{CT-LE} = 0.75$) and weak LE–CT mixing, whereas **Encap-TAT** has a smaller gap ($E_{CT} \approx 2.85$ eV; $E_{LE} \approx 2.50$ eV; $\Delta E_{CT-LE} = 0.35$ eV) and stronger hybridisation. By mapping their optical signatures and fission dynamics, we show how increasing bridge resonance can either support long-lived triplets via CT-assisted superexchange or suppress iSF through exciplex-like trapping.

Results and Discussion

Molecular Synthesis and Structures.

To investigate how bridge–chromophore CT state alignment modulates the intramolecular singlet fission (iSF) landscape, we compared two trimeric scaffolds, **TIPS-TAT** and **Encap-TAT** (Figure 2). Both architectures incorporate a TIPS-anthracene



ARTICLE

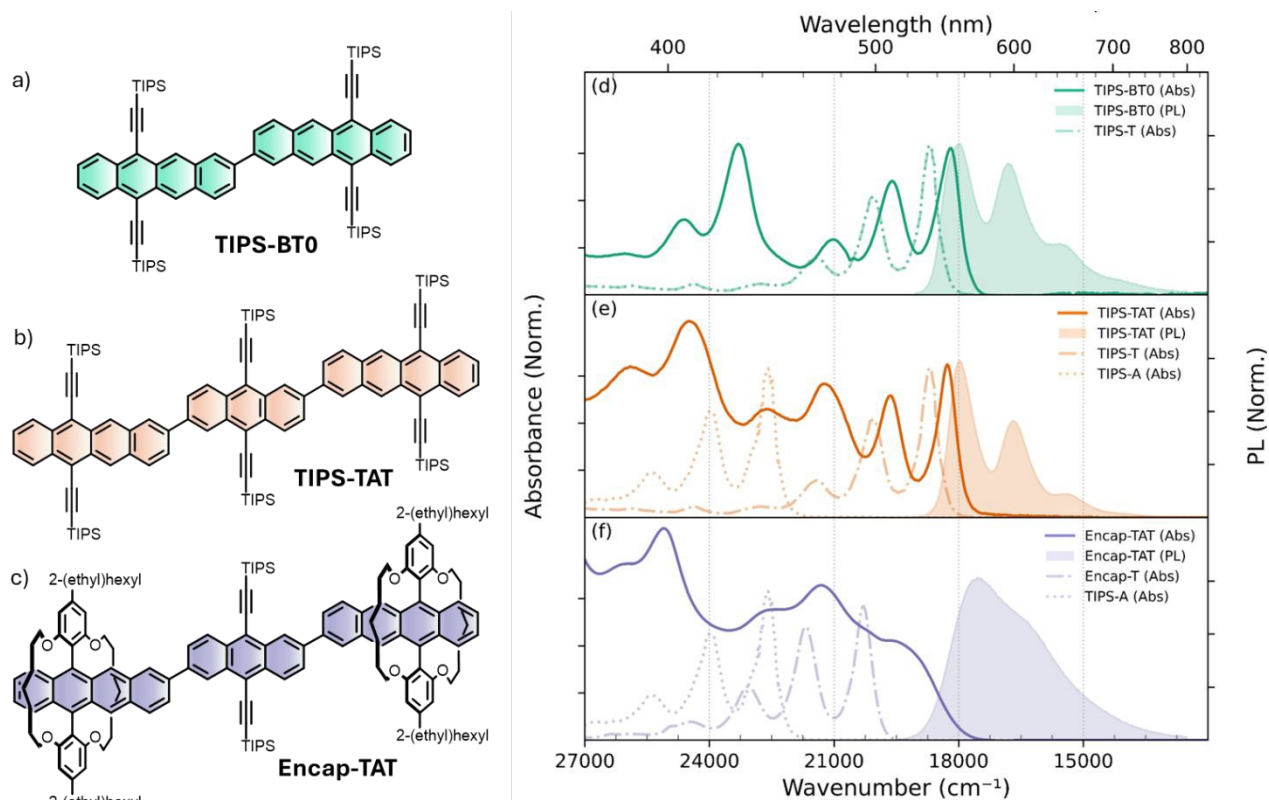


Figure 2. Chemical structures (left) of the dimer **TIPS-BTO** (a), the trimer **TIPS-TAT** (b), and the encapsulated trimer **Encap-TAT** (c). Panels (d–f) show normalized absorption and photoluminescence (PL) spectra (right) of chromophoric architecture in comparisons with its corresponding monomeric subunits. All absorption (solid lines) and PL (filled curves) spectra are recorded in dilute toluene solution ($\sim 20 \mu\text{M}$) at room temperature. The vibronic structure of **TIPS-T** is retained in **TIPS-BTO** and **TIPS-TAT**, while the pronounced spectral reshaping in **Encap-TAT** reflects strong electronic communication mediated through/with the central **TIPS-A** bridge. **TIPS**: triisopropylsilyl group

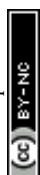
(**TIPS-A**) bridge, however, in **Encap-TAT** the local excited-state energy of the bridge is more closely aligned with that of the **Encap-Tetracene** (**Encap-T**) chromophores. In addition, the charge-transfer (CT) state in **Encap-TAT** lies energetically closer to the local exciton (LE) state compared to **TIPS-TAT**, thereby enhancing the possibility of LE-CT hybridization. The synthesis of the dimer **TIPS-BTO** (Figure 2a) and the trimer **TIPS-TAT** (Figure 2b) have been reported previously.^{51,53} Unlike the trimeric systems, **TIPS-BTO** is a directly linked **TIPS-tetracene** dimer without a bridging unit and thus serves as a baseline reference for iSF. Building on these precedents, **Encap-TAT** (Figure 2c) was prepared via a convergent route culminating in a Suzuki cross-coupling onto a rigid macrocyclic scaffold (Scheme S1–S3). The macrocycle was deliberately chosen to suppress aggregation and finely tune the energetic alignment between bridge and chromophore units.⁵² 2-(Ethyl)hexyl alkyl chains ensure sufficient solubility.

Across all three molecular architectures, from the dimer

TIPS-BTO to the trimers **TIPS-TAT** and **Encap-TAT**, DFT calculations suggest that the dihedral angle (θ) between each tetracene unit and adjacent arene units is consistently $\sim 32\text{--}33^\circ$ (Figure S1). This intrinsic twist and bulky solubilizing substituents suppress face-to-face $\pi\text{--}\pi$ stacking while retaining orbital overlap sufficient for electronic communication (Figure S2–S4). By combining structural rigidity with controlled connectivity, these scaffolds establish a well-defined platform for probing how bridge-mediated electronic alignment governs intramolecular singlet fission efficiency.

Steady-State Optical Characteristics and Bridge–Chromophore Excitonic Interaction

Figure 2 shows the normalized absorption (solid lines) and photoluminescence (PL, filled areas) spectra of the **TIPS-BTO**, **TIPS-TAT** and **Encap-TAT** trimer in dilute toluene ($c \approx 20 \mu\text{M}$). In the weak-to-intermediate coupling regime, where the electronic coupling J is small compared to the principal acene



vibrational quantum ($\hbar\omega \approx 1400 \text{ cm}^{-1}$), vibronic intensity ratios provide a more sensitive measure of excitonic delocalization than simple band shifts. In particular, the 0–0/0–1 ratio directly reflects exciton delocalization within a perturbative Franck–Condon excitation framework.^{54–56}

The **TIPS-BTO** dimer (Fig. 2a, 2d, Table S1) exhibits the canonical TIPS-tetracene vibronic progression, with a sharp 0–0 band near 550 nm (18,182 cm^{-1}) and a 0–1 shoulder at $\sim 510 \text{ nm}$ (19,608 cm^{-1}). Compared to the monomer, enhanced 0–1 intensity signals weak H-type excitonic coupling between the tetracene units. In addition, a modest red shift of the excitonic band ($\sim 500 \text{ cm}^{-1}$) and the emergence of a CT-derived absorption feature near 429 nm (23,310 cm^{-1}), which borrows oscillator strength through LE–CT mixing is observed.⁵⁷ This reveals the presence of LE–CT interactions mediated by frontier orbital overlap between the chromophores.^{58–60} The PL spectrum retains a well-resolved vibronic progression with a small Stokes shift ($\sim 196 \text{ cm}^{-1}$), confirming localized $S_1 \rightarrow S_0$ emission.

Building on this reference case, incorporation of a **TIPS-A** bridge in the **TIPS-TAT** trimer introduces new spectral features (Fig. 2e). The asymmetric architecture relaxes symmetry restrictions present in homodimers, allowing both the lower-energy ($S_0 \rightarrow S_1$) and higher-energy ($S_0 \rightarrow S_2$) transitions (Table S2–S3, Figure 1C).⁵⁷ The $S_0 \rightarrow S_1$ transition ($\sim 547 \text{ nm}$, 18,282 cm^{-1}), retains the tetracene vibronic progression but shows enhanced 0–1 intensity, consistent with weak H-type excitonic coupling mediated through/with the bridge and exhibits a modest red shift ($\sim 400 \text{ cm}^{-1}$) relative to the **TIPS-T** monomer. A distinct ($S_0 \rightarrow S_2$) band at 471 nm (21,230 cm^{-1}) is red-shifted by $\sim 471 \text{ cm}^{-1}$ relative to isolated **TIPS-A**, while a CT-derived band emerges near 408 nm with enhanced oscillator strength from LE–CT coupling.⁵⁷ Together, these signatures confirm appreciable orbital overlap across the trimer backbone and modest LE–CT mixing. The PL spectrum preserves the tetracene-like vibronic structure, indicating that despite through/with bridge interactions, emission remains dominated by localized **TIPS-T** excitons.

By contrast, **Encap-TAT** (Fig 2c, 2f and S5) displays qualitatively different optical behavior. Fusing **Encap-T** units that are more closely aligned in energy with the **TIPS-A** bridge erases monomeric vibronic progression, yielding a broad, vibronically unresolved absorption envelope (27,000–21,000 cm^{-1}). The PL spectrum is likewise broad, red-shifted, featureless with a large Stokes shift ($\sim 1932 \text{ cm}^{-1}$). These trends are consistent with a substantially reduced LE–CT separation in **Encap-TAT** ($\Delta E_{CT-LE} \approx 0.35$) relative to **TIPS-TAT** ($\approx 0.75 \text{ eV}$), which enhances LE–CT hybridisation and favors relaxation into an intramolecular exciplex-like minimum.^{56,61} Overall, the progression from **TIPS-TAT** to **Encap-TAT** shows that decreasing LE–CT separation drives increasingly strong hybridization, with **Encap-TAT**'s PL consistent with intramolecular excimer/exciplex-like emission.

Single-Arm Encap-TA: Isolating Bridge-Mediated Interactions.

To probe the origin of **Encap-TAT**'s distinctive optical response, we synthesized the single-arm **Encap-TA** dimer (Scheme S3) and

performed steady-state optical measurements to quantify bridge-chromophore interactions (Figure 3). As shown in Figure 3c, the normalized absorption (solid) and PL (dashed) spectra of **Encap-T** (monomer, black), **Encap-TA** (dimer, red), and **Encap-TAT** (trimer, blue) reveal a clear progression from a localized chromophore to an intermediate, single-arm dimer, and finally to a strongly LE–CT coupled trimer.

In contrast to the broadened, featureless absorption of **Encap-TAT**, **Encap-TA** displays a structured spectrum with well-resolved vibronic features. Two lower-energy peaks at $\sim 512 \text{ nm}$ (19,531 cm^{-1}) and $\sim 479 \text{ nm}$ (20,878 cm^{-1}), assigned to the $S_0 \rightarrow S_1$ progression (Table S4) are weaker than a higher-energy band at $\sim 453 \text{ nm}$ (22,076 cm^{-1}). This inversion of intensity reflects contributions from both S_1 and S_2 transitions and is consistent with an intermediate-coupling regime, moderate H-type excitonic coupling, together with differences in transition-dipole strengths for the **Encap-T** chromophore and the **TIPS-A** bridge (Figure S6 and Table S2). A modest red shift in both LE derived (Frenkel-type) bands, peak broadening, and the appearance of a CT feature near $\sim 385 \text{ nm}$ (25,974 cm^{-1}) further indicate LE–CT coupling (in the diabatic basis) that yields LE–CT mixing and appreciable bridge–chromophore electronic communication.^{61,62} Notably, relative to **Encap-TA**, the **Encap-TAT** trimer exhibits additional red shifts of the $S_0 \rightarrow S_1/S_2$ envelope and the CT band, signalling much stronger LE–CT hybridisation in the trimer.

While the **Encap-TA** absorption remains vibronically resolved, its PL collapses into a broad, featureless envelope that is markedly broader and more red-shifted than the monomer (Fig. 3c). The monomer's 0–0 fluorescence at $\sim 500 \text{ nm}$ (20,012 cm^{-1}) is only $\sim 7 \text{ nm}$ ($\sim 270 \text{ cm}^{-1}$) red-shifted from its 0–0 absorption, whereas the **Encap-TA** PL peaks at $\sim 555 \text{ nm}$ ($\sim 18,018 \text{ cm}^{-1}$), exhibiting a $\sim 43 \text{ nm}$ ($\sim 1,513 \text{ cm}^{-1}$) Stokes shift and loss of vibronic structure. These pronounced red shifts and broadened, structureless PL in both **Encap-TA** and **Encap-TAT** are consistent with emission from a relaxed excited-state minimum that lies below the initially prepared Franck–Condon bright state. This behaviour is characteristic of an intramolecular exciplex-like (CT-stabilised) emissive state, i.e., emission from an adiabatic surface with enhanced CT character upon structural/solvent relaxation.^{47,63–66}

The experimental absorption spectrum of heterodimer **Encap-TA** was quantitatively reproduced by a full vibronic Frenkel–exciton model (Figure 3f and see section 1.12 in ESI), which decomposes the response into lower (E_-) and upper (E_+) excitonic branches. The best fit was obtained using a transition-dipole ratio of $\mu_2/\mu_1 = 0.75$ and $J = 334 \text{ cm}^{-1}$. In a heterodimer, the loss of inversion symmetry “lights up” both excitons, so E_- and E_+ each carry oscillator strength (Figure 1c). By contrast, a symmetric homodimer supports one bright and one dark exciton (Figure S7).^{61,67–69} In our fit, E_- captures the red-shifted S_1 manifold (Table S2), while E_+ accounts for the enhanced exciton-like (LE-derived) higher-energy feature near $\sim 480 \text{ nm}$. The charge-transfer (CT) contribution is modelled as a single Lorentzian centered at $\sim 26,000 \text{ cm}^{-1}$ ($\sim 385 \text{ nm}$), shown as the purple dotted trace in Fig. 3d (Section 1.12, ESI).



ARTICLE

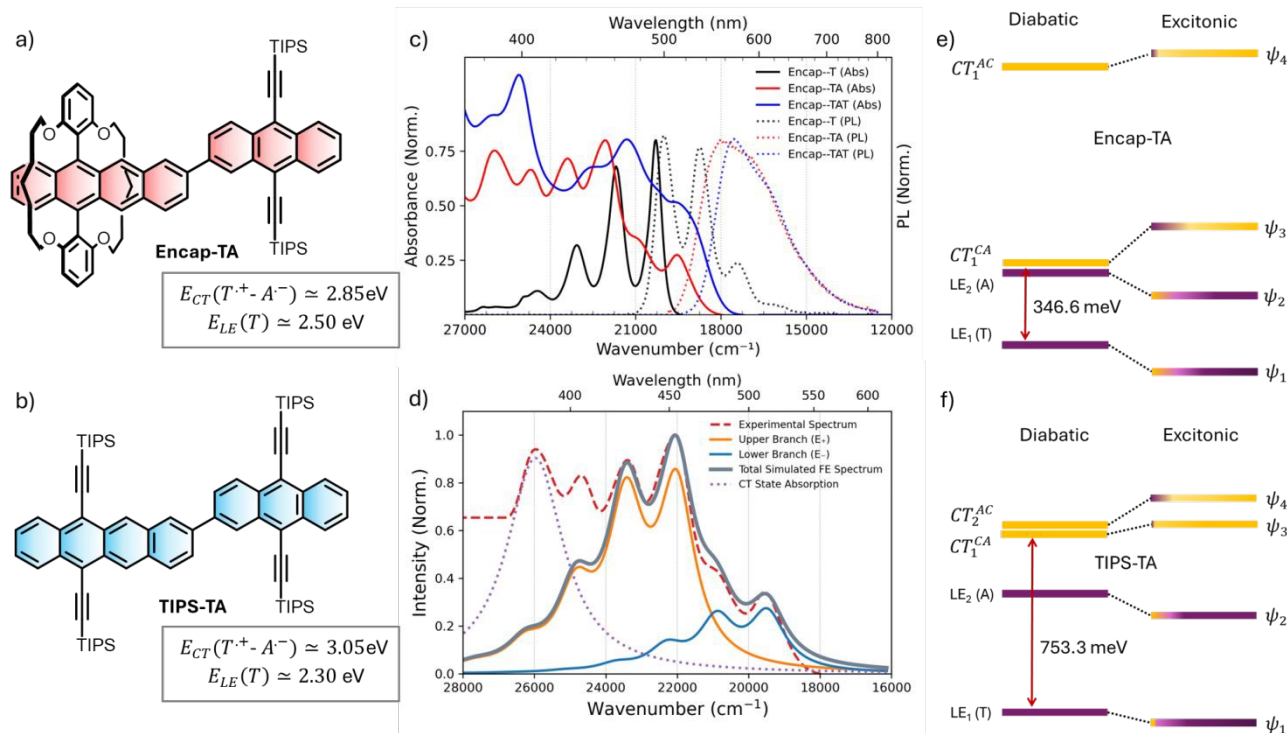


Figure 3. Molecular structure of the Encap-TA dimer (a), composed of an Encap-T chromophore covalently linked to a TIPS-A bridge and TIPS-TA dimer (b), featuring a direct connection between TIPS-T and TIPS-A units. (c) Normalized absorption (solid lines) and photoluminescence (PL) spectra (dotted lines) of the monomeric unit (Encap-T), dimer (Encap-TA), and trimer Encap-TAT, recorded in dilute toluene ($c \approx 20 \mu\text{M}$). (d) Experimental absorption spectrum of Encap-TA (gray) fitted using an exciton–vibrational coupling model, resolving contributions from the upper (E_+) and lower (E_-) excitonic branches, a CT-like state, and vibronically structured LE components. Schematic energy-level diagrams showing diabatic electronic states (LE and CT, before mixing) and the resulting adiabatic excitonic states (after mixing) for Encap-TA (e) and TIPS-TA (f). The adiabatic eigenstates (ψ_1 – ψ_4) are significant mixture of the underlying diabatic LE and CT states.

Quantifying LE–CT Mixing in Encap-TA and TIPS-TA.

To validate our spectroscopic assignments, we quantified LE–CT mixing in the **Encap-TA** and **TIPS-TA** dimers by constructing and diagonalising a four-state diabatic Hamiltonian in the localized configuration basis $\{|LE_A\rangle, |LE_B\rangle, |CT_{CA}\rangle, |CT_{AC}\rangle\}$, where $|CA\rangle \equiv A^+B^-$ and $|AC\rangle \equiv A^-B^+$ (section 1.8–1.11, ESI). Diagonalization results in four adiabatic states (ψ_1 – ψ_4) whose LE-subspace (excitonic) vs CT-subspace weights, obtained from the eigenvector coefficients, are reported in Table 1 and correlated with the spectra in Fig. 3e and 3f. In this Hamiltonian, LE–CT coupling is mediated by the electron- and hole-transfer integrals (t_e, t_h). In both dimers, t_e and t_h exceed the LE–LE Coulombic coupling (J_{Coul}), indicating that charge-mediated superexchange coupling rather than direct Coulomb coupling governs interunit communication (Table S5–S8). LE–CT mixing refers exclusively to the LE vs CT composition of these adiabatic eigenstates (ψ_1 – ψ_4).

For **Encap-TA** dimer, the two lowest adiabatic states are LE-dominant but carry substantial CT content ($\psi_1, \psi_2 \approx 83$ – 81% LE / 17 – 19% CT; Tables 1 and S9). Both are stabilized relative to their diabatic LE site energies (-804.0 cm^{-1} for ψ_1) and (-663.9 cm^{-1} for ψ_2), consistent with strong CT-mediated mixing and the red-shifted LE envelope (Figure 3e). Concomitantly, a nominal CT state (ψ_3) is mixed down and acquires appreciable LE character ($\sim 31\%$), evidencing pronounced LE–CT hybridization. In parallel, level repulsion destabilizes the diabatic CT manifold by several hundred cm^{-1} leaving the CT states high in energy yet optically active via LE–CT mixing. Despite the CT adiabats lying several thousand cm^{-1} above the LE manifold, this superexchange is sufficient to (i) stabilize the bright LE pair (spectral red shift), (ii) activate CT-derived absorption via oscillator-strength borrowing, and (iii) broaden/soften vibronic structure mirroring the observed absorption and PL trends of **Encap-TA** (and, amplified further, in **Encap-TAT**).



ARTICLE

Table 1. Energies and local-excitation (LE) vs charge-transfer (CT) composition of the adiabatic excited states formed upon diagonalization of a 4-state diabatic Hamiltonian. ψ_1 – ψ_4 denote eigenstates in ascending energy

State	TIPS-TA			Encap-TA		
	Energy (cm ⁻¹)	LE (%)	CT (%)	Energy (cm ⁻¹)	LE (%)	CT (%)
ψ_1	18,226.95	95.3	4.7	19,359.78	83.3	16.7
ψ_2	21,742.32	82.8	17.2	21,745.28	81.4	18.6
ψ_3	24,848.05	2.9	97.1	24,056.15	31.1	68.9
ψ_4	25,609.39	19.0	81.0	29,849.95	4.3	95.7

In contrast, **TIPS-TA** displayed weaker LE and CT mixing. ψ_1 remains highly localized (~95% LE) and ψ_2 shows only modest CT admixture (~17% CT), while the upper pair is largely CT-like (ψ_3 – $\psi_4 \approx 81$ –97% CT; Tables 1 and S10). Spectroscopically, optical features of the **TIPS-TAT** dimer are consistent with the electronic structure derived from the **TIPS-TA** model, comprising two stabilized LE-derived (exciton-like) absorption bands with only modest CT admixture, a weak intensity-borrowed CT band, and comparatively narrower vibronic signatures (Fig. 3f). The difference relative to **Encap-TA** arises from smaller effective LE-CT coupling and a larger LE-CT energy separation, which together suppress hybridization into the lowest bright states. Taken together, these results highlight starkly different mixing regimes. **Encap-TA** exhibits strong CT-mediated superexchange that injects appreciable CT character into the lowest LE-derived (exciton-like) adiabatic state, while **TIPS-TA** supports a more localized lowest state with only minor CT admixture.

Impact of LE-CT hybridisation on Intramolecular Singlet Fission

In this section, we investigate how strong excitonic hybridization between local exciton (LE) states and bridge-chromophore charge-transfer (CT) states reshape the excited-state manifold and perturb the kinetic landscape of intramolecular singlet fission. To probe these effects, we performed both femtosecond and nanosecond transient absorption (fs/nsTA) measurements on **TIPS-BTO**, **TIPS-TAT**, and **Encap-TAT** in toluene ($c \approx 100 \mu\text{M}$) at room temperature. Figure 4a, d, g shows the fsTA contour maps ($\Delta T/T$ as a function of probe wavelength and pump-probe delay) for the three systems following photoexcitation at 530 nm. Target/global analysis of the fsTA datasets using the kinetic schemes described in Section 1.7 in ESI yields the evolution- and species-associated spectra summarized in Figure 4.^{70,71}

Upon photoexcitation, **TIPS-BTO** (Fig. 4a–4c) exhibits the characteristic $S_1 \rightarrow S_n$ photoinduced absorption (PIA) bands of **TIPS-T** or tetracene dimer chromophores centered at ≈ 657 nm and ≈ 446 nm, accompanied by ground-state bleach (GSB)

features near ≈ 541 nm and ≈ 430 nm.^{48,72–74} Target analysis reveals that the initially populated S_1 state decays with a lifetime of 1.39 ± 0.03 ps, concomitant with the rise of a correlated triplet pair (^1TT) PIA, centred at 520 nm, spanning the 570–615 nm region as well as 657 nm. The ^1TT population persists beyond the temporal window of the fsTA measurement. In the nanosecond transient absorption (nsTA) data (Figure 5a, instrument response ≈ 1 –2 ns), the same ^1TT -associated PIA features are observed in the early time. These then decay monoexponentially with a lifetime of $\tau_{\text{TT}} \approx 8.7 \pm 0.4$ ns, ultimately leaving only a weak residual signal assigned to long-lived triplet (T_1) state PIA (Figures S8–S10). The absence of correlated triplet pair dissociation into free triplets ($^1\text{TT} \rightarrow 2T_1$) is attributed to strong electronic communication between the chromophores and a high triplet-triplet exchange interaction. This elevated exchange coupling stabilizes the bound ^1TT state and suppresses spin decoherence, thereby preventing its evolution into two non-interacting triplet excitons.^{75,76}

The fsTA response of the **TIPS-TAT** trimer shows qualitatively similar characteristic S_1 state features, $S_1 \rightarrow S_n$ PIA spanning from ~ 590 nm to 850 nm, a GSB centred around ~ 544 nm and prominent PIA bands below ~ 475 nm region (Figures 4d–4f and S11). While the singlet-state features resemble those of the monomer, the increased spectral broadening may arise from modest CT admixture / exciton-CT hybridisation in the initially accessed adiabatic manifold. Additionally, introducing a **TIPS-A** bridge that is closely aligned in energy substantially alters the ensuing excited-state kinetics. The rise of the ^1TT precursor in **TIPS-TAT**, tracked by PIA bands at 517 nm and 572–702 nm, occurs with $\tau_{\text{SF}} \approx 11.2 \pm 0.06$ ps, in line with the previous reports,^{28,51} but significantly slower than the 1.39 ps observed for **TIPS-BTO**. This deceleration reflects the longer centre-to-centre separation and added torsional flexibility introduced by the anthracene linker. Once formed, the ^1TT state in **TIPS-TAT** is remarkably long-lived ($\tau_{\text{TT}} \approx 127.56 \pm 1$ ns), $\sim 15\times$ longer than in the directly linked dimer and it undergoes partial separation of the correlated pair ($^1\text{TT} \rightarrow 2T_1$) to yield free triplets (Figures 5b, 5d and S12).

Quantitatively, from the fitted reversible $S_1 \rightleftharpoons ^1\text{TT}$ kinetics, we estimate correlated triplet-pair yields of $\phi_{\text{TT}} = 96.97\%$ (**TIPS-**



ARTICLE

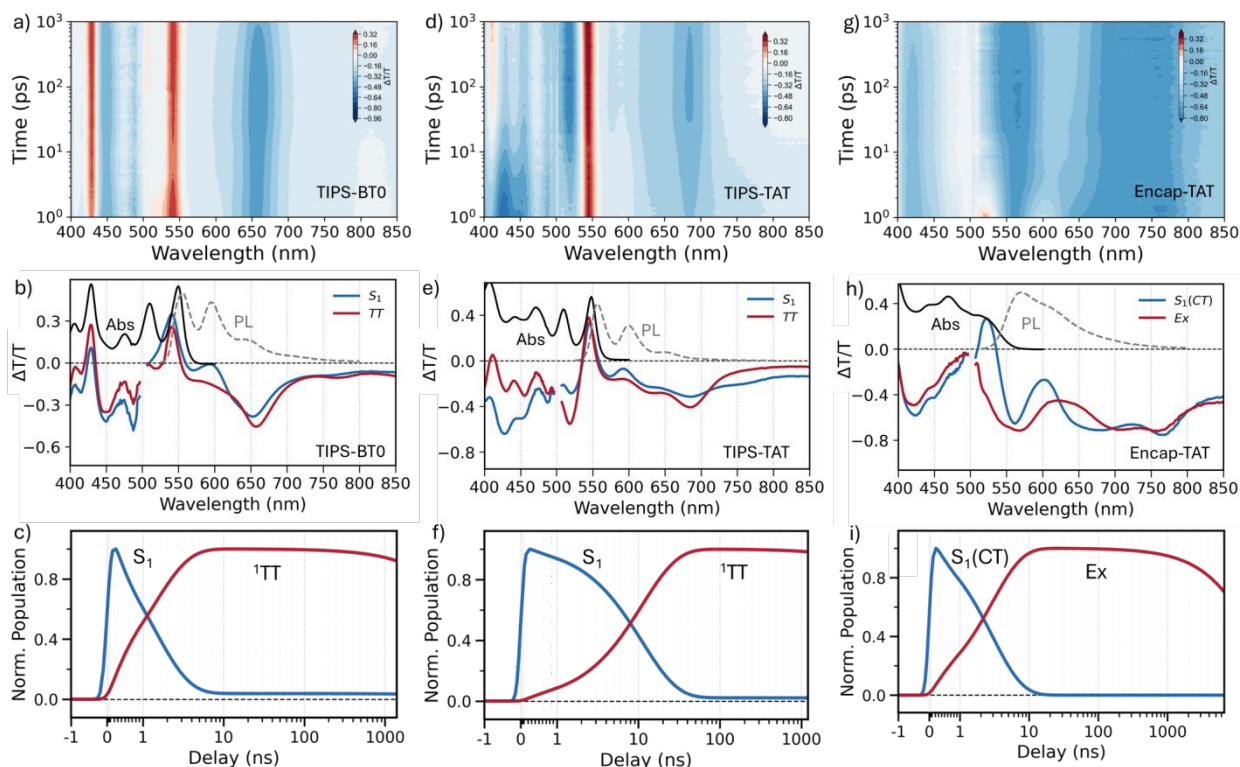


Figure 4. Femtosecond transient absorption (fsTA) spectra of TIPS-BTO (a), TIPS-TAT (d), and Encap-TAT (g) in toluene following 530 nm excitation, showing the evolution of the excited-state features as a function of delay time. Species-associated spectra (SAS) obtained from target analysis are for TIPS-BTO (b) and TIPS-TAT (e) while Evolution-associated difference spectra (EADS) obtained from global analysis are shown for Encap-TAT (h). The corresponding time-dependent species populations from the target/global analysis are shown in (c), (f), and (i) for TIPS-BTO, TIPS-TAT, and Encap-TAT, respectively.

BTO) and 98.02% (**TIPS-TAT**). Using the triplet-plateau analysis (SI Section 1.13), the yields of persistent isolated triplets are ~15.5% (**TIPS-BTO**) and ~58.8% (**TIPS-TAT**). Thus, while ^1TT formation is near-quantitative in both **TIPS-BTO** and **TIPS-TAT**, triplet separation is markedly more efficient in **TIPS-TAT**, underscoring the sensitivity of free-triplet generation to bridge-controlled exciton-CT mixing. This pronounced stabilization of the ^1TT manifold highlights how bridge-resonant coupling can both extend multiexciton lifetimes and boost free-triplet yields, even while moderating the initial fission rate. In the case of **TIPS-TAT**, the presence of the bridge reduces the triplet-triplet exchange interaction between the terminal **TIPS-T** units, thereby facilitating spin decoherence and promoting the formation of spatially separated, long-lived free triplets.

In stark contrast, **Encap-TAT** exhibits a fundamentally different early-time TA signature. Upon 530 nm excitation, its $S_1 \rightarrow S_0$ photoinduced absorption (PIA) no longer display well-resolved peaks characteristic of the monomer Encap-T (Figures 4g-4i and S13-S15). Instead, it emerges as a broad, red-shifted, structureless band spanning ≈ 550 -850 nm, with the ground-

state bleach confined to ≤ 525 nm. This simultaneously red-shifted, unstructured PIA is consistent with substantial CT admixture in the lowest adiabatic manifold, as quantified for **Encap-TA** (≈ 17 -19% CT) and expected to be enhanced in **Encap-TAT** given the smaller LE-CT detuning and stronger bridge-chromophore coupling. We therefore assign this feature to a singlet exciton with significant CT admixture, hereafter denoted as $S_1(\text{CT})$. The initially populated $S_1(\text{CT})$ feature decays with $\tau_{Ex} \approx 2.95 \pm 0.04$ ps into a second state whose PIA is broader and completely unstructured across the probe window. The decay of the initially populated state is markedly faster than in **TIPS-TAT**, and the resulting spectral profile closely resembles the intramolecular excimer-like states reported in related chromophoric systems.^{48,63-66,77,78} This markedly different from the well-defined ^1TT signature seen **TIPS-BTO** or **TIPS-TAT** and similar tetracene derivatives.^{7,73}

We therefore refer to this broad, unstructured transient state as an intramolecular exciplex-like state (Ex) under dilute conditions. Here, Ex denotes a relaxed minimum on an exciton-CT-hybrid adiabatic surface with substantial bridge-



chromophore CT character. We attribute Ex formation to structural and solvent relaxation on this hybrid surface, which progressively stabilises a more CT-rich minimum along the nuclear coordinate. Such relaxation can access a distribution of closely spaced relaxed minima (exciplex-like conformers) on the excited-state landscape, consistent with the progressive broadening and loss of vibronic structure observed in the

transient absorption.^{47,64} The Ex-state decays with lifetime of $\approx 16.9 \pm 0.2$ ns back to the ground state, leaving only a very weak residual PIA attributable to long-lived T_1 excitons (Figure S16 and Table S11). The assignment of this exciplex-like state, as a CT-stabilised relaxed minimum on an exciton-CT hybrid surface, is further supported by solvent-dependent steady-state photophysics. In **Encap-TAT**, the PL maximum exhibits a pronounced

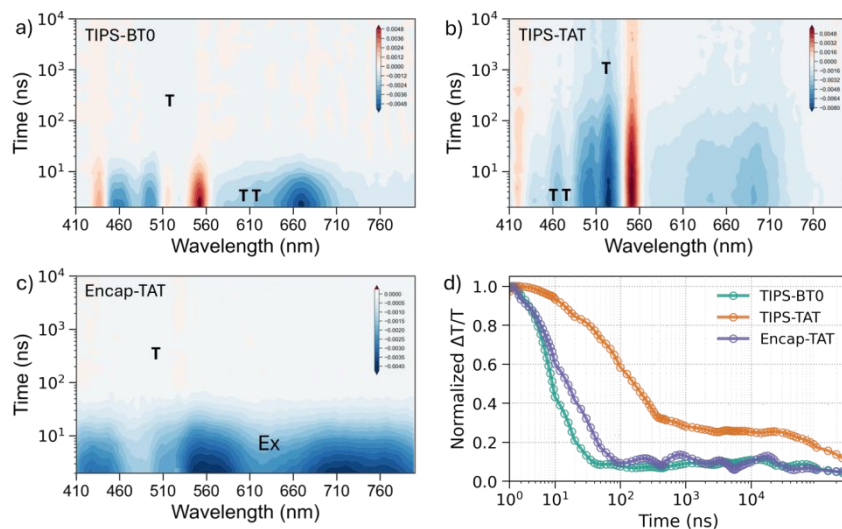


Figure 5. Nanosecond transient absorption (nsTA) data of TIPS-BTO (a), TIPS-TAT (b), and Encap-TAT (c) in toluene following 532 nm photoexcitation, highlighting the spectral signatures of free triplets (T), correlated triplet pair (1TT), and intramolecular exciplex state (Ex). (d) Corresponding kinetic traces monitored at the respective triplet PIA maxima: TIPS-BTO (480-510 nm), TIPS-TAT (500-520 nm), and Encap-TAT (470-500 nm), illustrating differences in triplet decay dynamics across the series

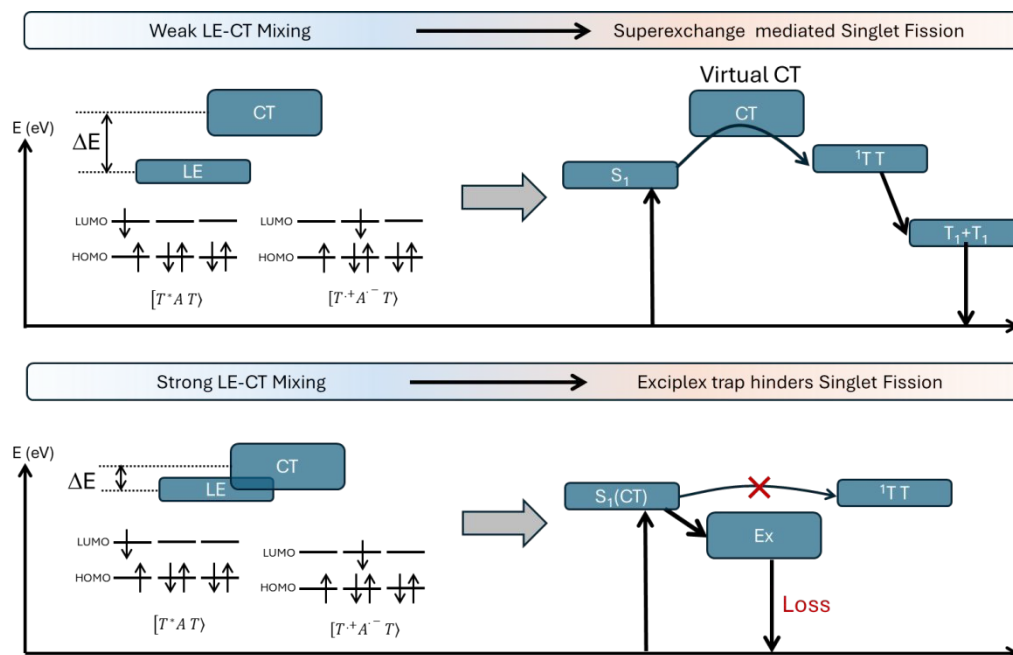


Figure 6. LE-CT mixing governs whether singlet fission proceeds by superexchange or is quenched by an exciplex trap. The schematic summarizes two limiting regimes controlled by the LE-CT detuning and coupling. Top (weak LE-CT mixing; superexchange-mediated singlet fission): when the LE state of the terminal SF chromophore is energetically well separated from the CT configuration ($A^{\cdot-}T^{\cdot+}$) CT remains largely virtual and mediates population transfer from S_1 to the correlated triplet pair 1TT , followed by formation of separated triplets (T_1+T_1). Bottom (strong LE-CT mixing; exciplex trap): when the LE and CT states are closer in energy and strongly coupled, substantial LE-CT hybridization yields a CT-enriched singlet $S_1(CT)$ that relaxes to an intramolecular exciplex-like minimum (Ex). This trap diverts population away from $S_1(CT)$ to 1TT (red cross) and increases the non-productive loss. Thus, by tuning the LE-CT energy gap and state mixing, triplet-pair formation can be controlled.



ARTICLE

red shift with increasing solvent polarity, whereas **TIPS-TAT** shows no such solvatochromic response (Figure S17). Polarity stabilises CT states and enhances LE-CT mixing, whereas higher concentrations can introduce intermolecular excimer/aggregation pathways. Accordingly, measurements were performed under dilute conditions ($c \approx 100 \mu\text{M}$) to minimise intermolecular contributions, and solvent-dependent TA data are provided in the SI (Section 4, Figures S18-S25) to support the CT-rich character of the Ex state. These solvent-dependent fsTA and nsTA measurements (SI Section 4, Figures S18-S25) show that increasing polarity accelerates Ex formation and shortens its lifetime for **Encap-TAT**. In contrast, for the SF-active **TIPS-TAT**, increasing polarity primarily accelerates ${}^1\text{TT}$ formation without inducing comparable long-time quenching.

To further clarify the nature of this second component, we directly compared **Encap-TAT** with its single-arm analogue, **Encap-TA** (Figure S26-30). In **Encap-TA**, the initially populated S_1 (CT) state decays in $\approx 2.25 \pm 0.06$ ps into an equally broad, featureless PIA band spanning the entire probe window, virtually identical in spectral shape and kinetics to the second component seen in **Encap-TAT**. This broad PIA then relaxes to the ground state with a long-lived residual ($\tau_2 \approx 16\text{--}18$ ns), consistent with a small population of free T_1 formed by intersystem crossing. Crucially, the close correspondence between **Encap-TA** and **Encap-TAT** excludes a conventional multiexciton (${}^1\text{TT}$) assignment, since the triplet of **TIPS-A** lies far too high in energy to sustain a bound triplet pair with **Encap-T**.

Instead, we ascribe both decay components to a strongly mixed LE-CT hybrid state, hereafter denoted as the intramolecular exciplex-like (Ex) state. This state arises from nuclear and structural relaxation in the excited state, aided by stabilization of the CT energy and significant electron- and hole-transfer integrals coupling the bridge and chromophores. These factors hybridise the local excitons with CT configurations into a continuous, unstructured excited-state manifold.^{56,79–82} Importantly, such strong LE-CT hybridization suppresses the formation of well-defined triplet pairs localized on the terminal **Encap-T** units. The Ex-state instead forms on ultrafast timescales, outcompeting correlated triplet-pair formation, while simultaneously enhancing radiative decay pathways. This is consistent with the higher photo-luminescence quantum yield observed for **Encap-TAT** (80.5%) compared to **TIPS-TAT** ($\sim 38.5\%$).

To rationalize the contrasting excited-state pathways, we summarize the role of LE-CT hybridization using the mechanistic schematic in Figure 6. Under weak LE-CT mixing (top), exemplified by **TIPS-TAT**, the CT configuration associated with the bridge–chromophore pair remains largely virtual and mediates population transfer from S_1 to the correlated triplet

pair ${}^1\text{TT}$ via a CT-assisted superexchange pathway, followed by formation of separated triplets (T_1+T_1). In contrast, under strong LE-CT mixing (bottom), exemplified by **Encap-TAT**, reduced LE-CT detuning and enhanced coupling yield a CT-enriched singlet $S_1(\text{CT})$ that relaxes into an intramolecular exciplex-like minimum (Ex). This trap diverts population away from ${}^1\text{TT}$ formation and increases non-productive loss, consistent with the broadened, red-shifted spectral signatures and pronounced solvatochromic PL red shift observed for **Encap-TAT**.

Conclusions

By constructing the **TIPS-BTO**→**TIPS-TAT**→**Encap-TAT** series and combining steady-state/ultrafast spectroscopy with a four-state LE/CT diabatic Hamiltonian analysis, we show that bridge–chromophore energetic alignment governs exciton–CT hybridisation in the adiabatic excited states and thereby dictates the photophysical outcome in intramolecular singlet fission (iSF). In **TIPS-TAT**, a larger LE-CT energy offset limits CT admixture while retaining sufficient LE↔CT coupling to enable CT-assisted superexchange into ${}^1\text{TT}$, yielding long-lived, separable triplets. Although both **TIPS-BTO** and **TIPS-TAT** exhibit near-quantitative correlated triplet-pair formation ($\phi_{TT} > 95\%$), the isolated triplet yield differs substantially ($\sim 16\%$ for **TIPS-BTO** vs $\sim 59\%$ for **TIPS-TAT**), demonstrating that triplet separation is highly sensitive to bridge-controlled exciton–CT mixing. In contrast, in **Encap-TAT** a smaller LE-CT gap increases CT character and stabilises a CT-rich exciplex-like relaxed minimum, which competes with and suppresses iSF. For device applications, iSF scaffolds should therefore be engineered to maintain a sufficient LE-CT offset (avoiding excessive CT stabilisation) while keeping LE↔CT coupling in the moderate regime that supports CT-mediated superexchange, alongside efficient pathways for triplet separation/harvesting. Overall, tuning the LE-CT energy gap and bridge–chromophore coupling strength provides a practical design lever to direct molecular assemblies toward either correlated triplet formation or exciplex-like relaxation and emission.

Author contributions

A.R. and H.B. conceived and supervised the project. E.S. carried out the experimental investigations, theoretical calculations and prepared the initial draft of the manuscript. J.W. performed the photoluminescence quantum yield (PLQY) measurements. D.G.C., J.R., S.M., O.M., and H.H. were involved in the synthesis and characterization of the materials. All authors contributed to the discussion of the results and to the final version of the manuscript. All authors have given approval to the final version of the manuscript. † These authors contributed equally



Conflicts of interest

All experimental/computational data and procedures are available in the ESI.†.

Data availability

The data underlying all figures and tables in this article are publicly available from the University of Cambridge repository at https://doi.org/DOI_TO_BE_ADDED_IN_PROOFS. This repository includes the underlying datasets and the analysis outputs used to generate the figures. Any analysis code and scripts used for data processing, fitting, and figure generation are also available in the same repository. Additional supporting data are provided in the Supplementary Information.

Acknowledgements

E.S. acknowledge funding from UKRI Postdoctoral Individual Fellowships (Grant No. EP/Y026659/1). D.G.C. Would like to acknowledge the Herchel Smith Fund for an early career fellowship, and the Royal Society (URF\R1\241806). L.M.C. thanks the U.S. Department of Energy, Office of Science, Office of Basic Energy Sciences for funding under Award Number DE-SC0022036. This work was supported by a UKRI Frontier Research Grant (EP/Y015584/1) and by an Engineering Physical Sciences Research Council Programme Grant (EP/W017091/1).

References

- 1 D. N. Congreve, J. Lee, N. J. Thompson, E. Hontz, S. R. Yost, P. D. Reusswig, M. E. Bahlke, S. Reineke, T. Van Voorhis and M. A. Baldo, *Science* (1979), 2013, **340**, 334–337.
- 2 M. B. Smith and J. Michl, *Chem. Rev.*, 2010, **110**, 6891–6936.
- 3 A. Rao and R. H. Friend, *Nat. Rev. Mater.*, 2017, **2**, 1–12.
- 4 J. Xia, S. N. Sanders, W. Cheng, J. Z. Low, J. Liu, L. M. Campos, T. J. Sun Xia, W. Cheng, J. Liu, T. Sun, S. N. Sanders, J. Z. Low, L. M. Campos and J. Xia, *Advanced Materials*, 2017, **29**, 1601652.
- 5 A. Kunzmann, M. Gruber, R. Casillas, J. Zirzmeier, M. Stanzel, W. Peukert, R. Tykwinski and D. M. Guldi, *Angewandte Chemie International Edition*, 2018, **57**, 10742–10747.
- 6 O. V. Mikhnenko, P. W. M. Blom and T. Q. Nguyen, *Energy Environ. Sci.*, 2015, **8**, 1867–1888.
- 7 S. T. Roberts, R. E. McAnally, J. N. Mastron, D. H. Webber, M. T. Whited, R. L. Brutchey, M. E. Thompson and S. E. Bradforth, *J. Am. Chem. Soc.*, 2012, **134**, 6388–6400.
- 8 S. W. Eaton, L. E. Shoer, S. D. Karlen, S. M. Dyar, E. A. Margulies, B. S. Veldkamp, C. Ramanan, D. A. Hartzler, S. Savikhin, T. J. Marks and M. R. Wasielewski, *J. Am. Chem. Soc.*, 2013, **135**, 14701–14712.
- 9 B. S. Basel, J. Zirzmeier, C. Hetzer, B. T. Phelan, M. D. Krzyaniak, S. R. Reddy, P. B. Coto, N. E. Horwitz, R. M. Young, F. J. White, F. Hampel, T. Clark, M. Thoss, R. R. Tykwinski, M. R. Wasielewski and D. M. Guldi, *Nat. Commun.*, 2017, **8**, 1–8.
- 10 S. N. Sanders, E. Kumarasamy, A. B. Pun, M. T. Trinh, B. Choi, J. Xia, E. J. Taffet, J. Z. Low, J. R. Miller, X. Roy, X. Y. Zhu, M. L. Steigerwald, M. Y. Sfeir and L. M. Campos, *J. Am. Chem. Soc.*, 2015, **137**, 8965–8972.
- 11 J. Kim, D. C. Bain, V. Ding, K. Majumder, D. Windemuller, J. Feng, J. Wu, S. Patil, J. Anthony, W. Kim and A. J. Musser, *Nat. Chem.*, 2024, **16**, 1680–1686.
- 12 K. C. Krishnapriya, P. Roy, B. Puttaraju, U. Salzner, A. J. Musser, M. Jain, J. Dasgupta and S. Patil, *Nat. Commun.*, 2019, **10**, 1–8.
- 13 G. He, E. M. Churchill, K. R. Parenti, J. Zhang, P. Narayanan, F. Namata, M. Malkoch, D. N. Congreve, A. Cacciuto, M. Y. Sfeir and L. M. Campos, *Nature Communications* 2023 14:1, 2023, **14**, 1–10.
- 14 E. Busby, J. Xia, Q. Wu, J. Z. Low, R. Song, J. R. Miller, X. Y. Zhu, L. M. Campos and M. Y. Sfeir, *Nat. Mater.*, 2015, **14**, 426–433.
- 15 A. B. Pun, S. N. Sanders, E. Kumarasamy, M. Y. Sfeir, D. N. Congreve, L. M. Campos, A. B. Pun, S. N. Sanders, E. Kumarasamy, L. M. Campos, M. Y. Sfeir and D. N. Congreve, *Advanced Materials*, 2017, **29**, 1701416.
- 16 T. Yamakado, S. Takahashi, K. Watanabe, Y. Matsumoto, A. Osuka, S. Saito, T Yamakado, J S Takahashi, K. W. Atanabe, Y. M. Atsumoto, P. R. A. Osuka and S. Saito, *Angewandte Chemie International Edition*, 2018, **57**, 5438–5443.
- 17 L. Schaufelberger, J. T. Blaskovits, R. Laplaza, K. Jorner and C. Corminboeuf, *Angewandte Chemie International Edition*, 2025, **64**, e202415056.
- 18 S. Nakamura, H. Sakai, M. Fuki, R. Ooie, F. Ishiwari, A. Saeki, N. V. Tkachenko, Y. Kobori and T. Hasobe, *Angewandte Chemie International Edition*, 2023, **62**, e202217704.
- 19 A. M. Levine, G. He, G. Bu, P. Ramos, F. Wu, A. Soliman, J. Serrano, D. Pietraru, C. Chan, J. D. Batteas, M. Kowalczyk, S. J. Jang, B. L. Nannenga, M. Y. Sfeir, E. H. R. Tsai and A. B. Braunschweig, *Journal of Physical Chemistry C*, 2021, **125**, 12207–12213.
- 20 A. B. Pun, A. Asadpoordarvish, E. Kumarasamy, M. J. Y. Tayebjee, D. Niesner, D. R. McCamey, S. N. Sanders, L. M. Campos and M. Y. Sfeir, *Nature Chemistry* 2019 11:9, 2019, **11**, 821–828.
- 21 Y. Hong, M. Rudolf, M. Kim, J. Kim, T. Schembri, A. M. Krause, K. Shoyama, D. Bialas, M. I. S. Röhr, T. Joo, H. Kim, D. Kim and F. Würthner, *Nature Communications* 2022 13:1, 2022, **13**, 1–11.
- 22 T. Ullrich, P. Pinter, J. Messelberger, P. Haines, R. Kaur, M. M. Hansmann, D. Munz and D. M. Guldi, *Angewandte Chemie*, 2020, **132**, 7980–7988.
- 23 E. A. Margulies, Y. L. Wu, P. Gawel, S. A. Miller, L. E. Shoer, R. D. Schaller, F. Diederich and M. R. Wasielewski, *Angewandte Chemie International Edition*, 2015, **54**, 8679–8683.
- 24 C. Hetzer, D. M. Guldi and R. R. Tykwinski, *Chemistry - A European Journal*, 2018, **24**, 8245–8257.
- 25 B. S. Basel, R. M. Young, M. D. Krzyaniak, I. Papadopoulos, C. Hetzer, Y. Gao, N. T. La Porte, B. T. Phelan, T. Clark, R. R. Tykwinski, M. R. Wasielewski and D. M. Guldi, *Chem. Sci.*, 2019, **10**, 11130–11140.
- 26 E. A. Margulies, C. E. Miller, Y. Wu, L. Ma, G. C. Schatz, R. M. Young and M. R. Wasielewski, *Nat. Chem.*, 2016, **8**, 1120–1125.
- 27 M. J. Y. Tayebjee, S. N. Sanders, E. Kumarasamy, L. M. Campos, M. Y. Sfeir and D. R. McCamey, *Nat. Phys.*, 2017, **13**, 182–188.
- 28 K. R. Parenti, R. Chesler, G. He, P. Bhattacharyya, B. Xiao, H. Huang, D. Malinowski, J. Zhang, X. Yin, A. Shukla, S. Mazumdar, M. Y. Sfeir and L. M. Campos, *Nat. Chem.*, 2023, **15**, 339–346.



Journal Name

ARTICLE

- 29 T. Wang, H. Liu, X. Wang, L. Tang, J. Zhou, X. Song, L. Lv, W. Chen, Y. Chen and X. Li, *J. Mater. Chem. A Mater.*, 2023, **11**, 8515–8539.
- 30 W. Kim and A. J. Musser, *Adv. Phys. X*, 2021, **6**, 1918022.
- 31 W. B. Davis, W. A. Svec, M. A. Ratner and M. R. Wasielewski, *Nature*, 1998, **396**, 60–63.
- 32 K. Majumder, S. Mukherjee, J. Park, W. Kim, A. J. Musser and S. Patil, *Angewandte Chemie International Edition*, 2024, **63**, e202408615.
- 33 M. Majdecki, C. H. Hsu, C. H. Wang, E. H. C. Shi, M. Zakrocka, Y. C. Wei, B. H. Chen, C. H. Lu, S. Da Yang, P. T. Chou and P. Gawel, *Angewandte Chemie - International Edition*, 2024, **63**, e202401103.
- 34 E. Kumarasamy, S. N. Sanders, M. J. Y. Tayebjee, A. Asadpoordarvish, T. J. H. Hele, E. G. Fuemmeler, A. B. Pun, L. M. Yablou, J. Z. Low, D. W. Paley, J. C. Dean, B. Choi, G. D. Scholes, M. L. Steigerwald, N. Ananth, D. R. McCamey, M. Y. Sfeir and L. M. Campos, *J. Am. Chem. Soc.*, 2017, **139**, 12488–12494.
- 35 T. Wang, S. Zhang, Y. T. Ding, B. Y. Zhang, B. Yu, R. Xu, Z. X. Liu, C. L. Sun, C. Zhang, Q. Wang and H. L. Zhang, *J. Mater. Chem. C Mater.*, 2025, **13**, 9576–9583.
- 36 T. C. Berkelbach, M. S. Hybertsen and D. R. Reichman, *Journal of Chemical Physics*, 2013, **138**, 114103.
- 37 B. S. Basel, C. Hetzer, J. Zirzmeier, D. Thiel, R. Guldi, F. Hampel, A. Kahnt, T. Clark, D. M. Guldi and R. R. Tykwinski, *Chem. Sci.*, 2019, **10**, 3854–3863.
- 38 L. C. Lin, T. Smith, Q. Ai, B. K. Rugg, C. Risko, J. E. Anthony, N. H. Damrauer and J. C. Johnson, *Chem. Sci.*, 2023, **14**, 11554–11565.
- 39 B. Carlotti, I. K. Madu, H. Kim, Z. Cai, H. Jiang, A. K. Muthike, L. Yu, P. M. Zimmerman and T. Goodson, *Chem. Sci.*, 2020, **11**, 8757–8770.
- 40 H. M. Bergman, G. R. Kiel, R. J. Witzke, D. P. Nenon, A. M. Schwartzberg, Y. Liu and T. D. Tilley, *J. Am. Chem. Soc.*, 2020, **142**, 19850–19855.
- 41 D. Bansal, A. Kundu, V. P. Singh, A. K. Pal, A. Datta, J. Dasgupta and P. Mukhopadhyay, *Chem. Sci.*, 2022, **13**, 11506–11512.
- 42 W. Ishii, M. Fuki, E. M. Bu Ali, S. Sato, B. Parmar, A. Yamauchi, C. H. Mulyadi, M. Uji, S. Medina Rivero, G. Watanabe, J. Clark, Y. Kobori and N. Yanai, *J. Am. Chem. Soc.*, 2024, **146**, 25527–25535.
- 43 A. Mohanty, V. P. Singh, C. M. Hussain, M. Dey, D. Ghosh, P. Mukhopadhyay and J. Dasgupta, *Chem. Sci.*, 2025, **16**, 21368–21378.
- 44 A. Neef, S. Beaulieu, S. Hammer, S. Dong, J. Maklar, T. Pincelli, R. P. Xian, M. Wolf, L. Rettig, J. Pflaum and R. Ernstorfer, *Nature* 2023 **616**:7956, 2023, **616**, 275–279.
- 45 H. Miyamoto, K. Okada, K. Tada, R. Kishi and Y. Kitagawa, *Molecules*, 2024, **29**, 5449.
- 46 Y. Bo, Y. Hou, D. A. X. Lavergne, T. Clark, M. J. Ferguson, R. R. Tykwinski and D. M. Guldi, *Nature Communications* 2025 **16**:1, 2025, **16**, 1–12.
- 47 Y. J. Bae, D. Shimizu, J. D. Schultz, G. Kang, J. Zhou, G. C. Schatz, A. Osuka and M. R. Wasielewski, *Journal of Physical Chemistry A*, 2020, **124**, 8478–8487.
- 48 C. B. Dover, J. K. Gallaher, L. Frazer, P. C. Tapping, A. J. Petty, M. J. Crossley, J. E. Anthony, T. W. Kee and T. W. Schmidt, *Nature Chemistry* 2018 **10**:3, 2018, **10**, 305–310.
- 49 X. Feng and A. I. Krylov, *Physical Chemistry Chemical Physics*, 2016, **18**, 7751–7761.
- 50 S. Valianti and S. S. Skourtis, *Journal of Physical Chemistry Letters*, 2022, **13**, 939–946.
View Article Online
DOI: 10.1039/D6SC00278A
- 51 K. R. Parenti, G. He, S. N. Sanders, A. B. Pun, E. Kumarasamy, M. Y. Sfeir and L. M. Campos, *Journal of Physical Chemistry A*, 2020, **124**, 9392–9399.
- 52 J. Royakkers, A. Minotto, D. G. Congrave, W. Zeng, A. Patel, A. D. Bond, D. K. Bučar, F. Cacialli and H. Bronstein, *Journal of Organic Chemistry*, 2020, **85**, 207–214.
- 53 A. B. Pun, S. N. Sanders, M. Y. Sfeir, L. M. Campos and D. N. Congreve, *Chem. Sci.*, 2019, **10**, 3969–3975.
- 54 K. A. Kistler, C. M. Pochas, H. Yamagata, S. Matsika and F. C. Spano, *Journal of Physical Chemistry B*, 2012, **116**, 77–86.
- 55 F. Gao, Y. Zhao and W. Liang, *Journal of Physical Chemistry B*, 2011, **115**, 2699–2708.
- 56 N. J. Hestand and F. C. Spano, *Chem. Rev.*, 2018, **118**, 7069–7163.
- 57 T. J. H. Hele, E. G. Fuemmeler, S. N. Sanders, E. Kumarasamy, M. Y. Sfeir, L. M. Campos and N. Ananth, *Journal of Physical Chemistry A*, 2019, **123**, 2527–2536.
- 58 E. Sebastian and M. Hariharan, *J. Am. Chem. Soc.*, 2021, **143**, 13769–13781.
- 59 N. J. Hestand and F. C. Spano, *Acc. Chem. Res.*, 2017, **50**, 341–350.
- 60 N. J. Hestand and F. C. Spano, *Journal of Chemical Physics*, 2015, **143**, 244707.
- 61 D. Bialas, C. Brüning, F. Schlosser, B. Fimmel, J. Thein, V. Engel and F. Würthner, *Chemistry – A European Journal*, 2016, **22**, 15011–15018.
- 62 P. Ottiger, H. Köppel and S. Leutwyler, *Chem. Sci.*, 2015, **6**, 6059–6068.
- 63 R. Jing, Y. Li, K. Tajima, Y. Wan, N. Fukui, H. Shinokubo, Z. Kuang and A. Xia, *J. Phys. Chem. Lett.*, 2024, **15**, 1469–1476.
- 64 E. Sebastian, J. Sunny and M. Hariharan, *Chem. Sci.*, 2022, **13**, 10824–10835.
- 65 R. M. Young and M. R. Wasielewski, *Acc. Chem. Res.*, 2020, **53**, 1957–1968.
- 66 J. Hoche, M. Flock, X. Miao, L. N. Philipp, M. Wenzel, I. Fischer and R. Mitric, *Chem. Sci.*, 2021, **12**, 11965–11975.
- 67 S. F. Völker, A. Schmiedel, M. Holzapfel, K. Renziehausen, V. Engel and C. Lambert, *Journal of Physical Chemistry C*, 2014, **118**, 17467–17482.
- 68 J. Seibt, P. Marquetand, V. Engel, Z. Chen, V. Dehm and F. Würthner, *Chem. Phys.*, 2006, **328**, 354–362.
- 69 E. Kirchner, D. Bialas and F. Würthner, *Chemistry – A European Journal*, 2019, **25**, 11294–11301.
- 70 J. J. Snellenburg, S. Laptinok, R. Seger, K. M. Mullen and I. H. M. van Stokkum, *J. Stat. Softw.*, 2012, **49**, 1–22.
- 71 I. H. M. Van Stokkum, D. S. Larsen and R. Van Grondelle, *Biochimica et Biophysica Acta (BBA) - Bioenergetics*, 2004, **1657**, 82–104.
- 72 H. L. Stern, A. J. Musser, S. Gelinan, P. Parkinson, L. M. Herz, M. J. Bruzek, J. Anthony, R. H. Friend and B. J. Walker, *Proc. Natl. Acad. Sci. U. S. A.*, 2015, **112**, 7656–7661.
- 73 Z. Wang, H. Liu, X. Xie, C. Zhang, R. Wang, L. Chen, Y. Xu, H. Ma, W. Fang, Y. Yao, H. Sang, X. Wang, X. Li and M. Xiao, *Nat. Chem.*, 2021, **13**, 559–567.



ARTICLE

Journal Name

- 74 Y. Bo, Y. Hou, D. Thiel, R. Weiß, T. Clark, M. J. Ferguson, R. R. Tykwinski and D. M. Guldi, *J. Am. Chem. Soc.*, 2023, **145**, 18260–18275.
- 75 O. Millington, S. Montanaro, A. Sharma, S. A. Dowland, J. Winkel, J. Grune, A. Leventis, T. Bennett, J. Shaikh, N. Greenham, A. Rao and H. Bronstein, *J. Am. Chem. Soc.*, 2024, **146**, 29664–29674.
- 76 V. Abraham and N. J. Mayhall, *Journal of Physical Chemistry Letters*, 2021, **12**, 10505–10514.
- 77 R. A. Krueger and G. Blanquart, *J. Phys. Chem. A*, 2019, **123**, 1796–1806.
- 78 J. Choi, S. Kim, M. Ahn, J. Kim, D. W. Cho, D. Kim, S. Eom, D. Im, Y. Kim, S. H. Kim, K. R. Wee and H. Ihee, *Commun. Chem.*, 2023, **6**, 1–11.
- 79 N. J. Hestand, H. Yamagata, B. Xu, D. Sun, Y. Zhong, A. R. Harutyunyan, G. Chen, H. L. Dai, Y. Rao and F. C. Spano, *Journal of Physical Chemistry C*, 2015, **119**, 22137–22147.
- 80 H. Yamagata, J. Norton, E. Hontz, Y. Olivier, D. Beljonne, J. L. Brédas, R. J. Silbey and F. C. Spano, *Journal of Chemical Physics*, 2011, **134**, 204703.
- 81 S. Lukman, K. Chen, J. M. Hodgkiss, D. H. P. Turban, N. D. M. Hine, S. Dong, J. Wu, N. C. Greenham and A. J. Musser, *Nature Communications* 2016 7:1, 2016, **7**, 1–13.
- 82 Y. Ishino, K. Miyata, T. Sugimoto, K. Watanabe, Y. Matsumoto, T. Uemura and J. Takeya, *Physical Chemistry Chemical Physics*, 2014, **16**, 7501–7512.

View Article Online
DOI: 10.1039/D6SC00278A

Open Access Article. Published on 23 March 2026. Downloaded on 4/13/2026 2:32:02 AM.
This article is licensed under a Creative Commons Attribution-NonCommercial 3.0 Unported Licence.



Chemical Science Accepted Manuscript

Data availability

View Article Online
DOI: 10.1039/D6SC00278A

The data underlying all figures and tables in this article are publicly available from the University of Cambridge repository at https://doi.org/DOI_TO_BE_ADDED_IN_PROOFS. This repository includes the underlying datasets and the analysis outputs used to generate the figures. Any analysis code and scripts used for data processing, fitting, and figure generation are also available in the same repository. Additional supporting data are provided in the Supplementary Information.

